Design of Ellipsoid and Spherical Combined Light Source for Uniform Flux and Color Mixing

Rui-Min Zeng
Ze-Tian Tang
Cheng-Xi Xia
Yang Wang
Shan Jin
Xin Ren
Li-Feng Bian
Zhao Ding
Chen Yang, *Member, IEEE*
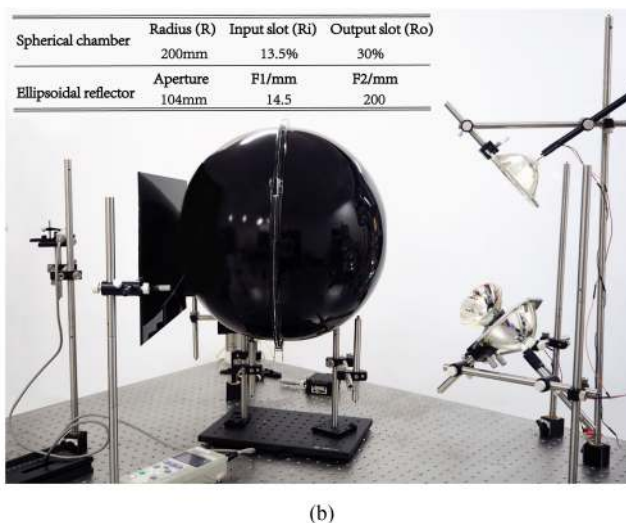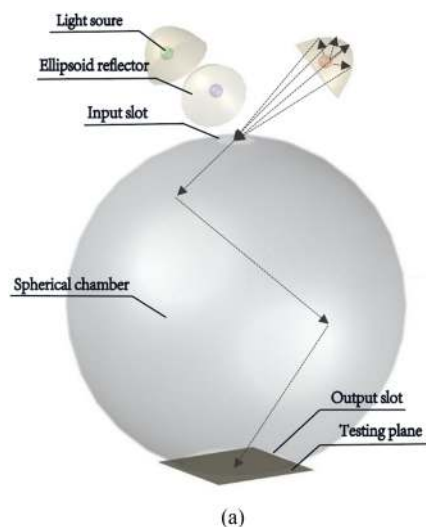
Spherical chamber	Radius (R)	Input slot (Ri)	Output slot (Ro)
	200mm	13.5%	30%
Ellipsoidal reflector	Aperture	F1/mm	F2/mm
	104mm	14.5	200

(a)   (b)

Design of Ellipsoid and Spherical Combined Light Source for Uniform Flux and Color Mixing

Rui-Min Zeng,[1] **Ze-Tian Tang,**[1] **Cheng-Xi Xia,**[1] **Yang Wang,**[1]
Shan Jin,[2,3] **Xin Ren,**[2] **Li-Feng Bian,**[2] **Zhao Ding,**[1]
and Chen Yang ⬡**,**[1] *Member, IEEE*

[1]College of Big Data and Information Engineering, Guizhou Key Laboratory of Micro-Nano
Electronics and Software Technology, Engineering Center of the Ministry of Education of
Semiconductor Power Device Reliability, Guizhou University, Guiyang 550025, China
[2]Key Laboratory of Nanodevices and Applications, Suzhou Institute of Nano-Tech and
Nano-Bionics, Chinese Academy of Sciences, Suzhou 215123, China
[3]School of Nano Technology and Nano Bionics, University of Science and Technology of
China, Hefei 230026, China

Abstract: In this letter, an ellipsoid–spherical combined light source structure is presented
for the purpose of uniform flux and color mixing, when considering heat dissipation. To allow
more rays couple into spherical chamber while keeping illumination uniformity, algebraic
equations to estimate light spot size focused by ellipsoidal reflector are derived and then
employed to decide input slot size of the chamber. Then Monte Carlo ray tracing simulation
suggests that the most preferable output slot size is between 15% and 30% of the chamber
radius when considering both uniformity and available test area. A prototype with a 150-W
Xenon arc lamp is fabricated to demonstrate heat distribution for the system, and experiment
about uniformity indicates that 89.4% of the test circle radius can reach 2% nonuniformity.
Color mixing performance for the system is studied by equipped with three ellipsoidal re-
flectors to collect rays from different color LEDs, and experiment shows that the maximum
root-mean-square error of the spectrum across 90% of output circle radius is 1.4%. Results
demonstrate it is a structure with simplified design process and having less dependence
with light source type.

Index Terms: Uniformity, color mixing, heat dissipation, nonimaging optics.

1. Introduction

Illumination uniformity is essential requirement for applications such display, solar simulators and
illumination sources in systems such as architecture [1], computer vision algorithms [2], and biomed-
ical systems [3]. For these application scenarios, nonuniformity can cause negative effects such
as partial shading, glare, and measurement uncertainty. Color mixing capabilities are sometimes
required to extend applications of the uniform illumination sources to provide stable or tunable light
spectrum for high quality test environment [4], [5].

Two main focuses of optimizing illumination systems to achieve uniform flux and provide rich
colors are light sources and optical path design, as reported in numerous literatures. For light
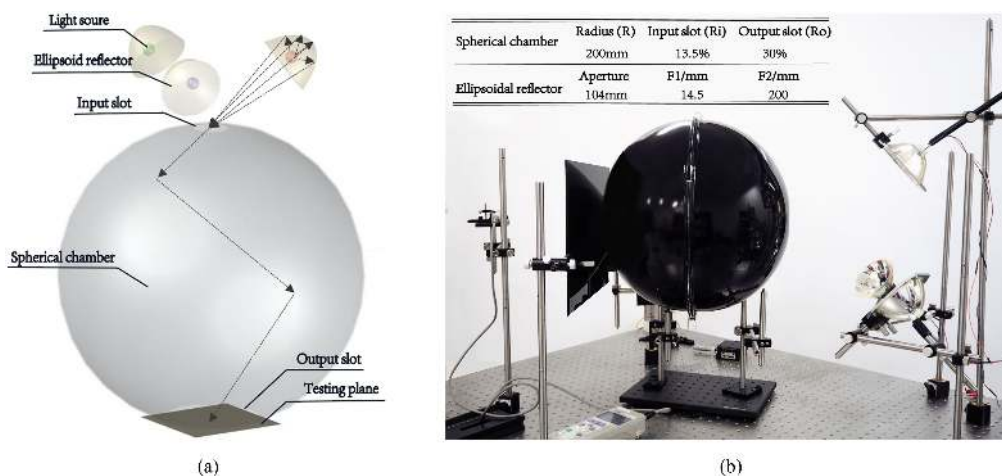
Fig. 1. Ellipsoid-spherical combined illumination system structure: (a) 3D schematic diagram, and (b) prototype of the structure.

sources, various types of the sources have been adopted according to the design requirement, such as high-pressure sodium lamp [6], quartz tungsten halogen lamp [7], [8], and metal halide lamp [9]–[12]. In particular, Xenon arc lamps have been widely used due to high output flux and match to solar spectrum [13]–[15]. Light emitting diodes (LEDs) are now becoming good candidates of uniformity illumination systems for their low cost, high stability, high efficiency, low heat dissipation, compact size and diverse spectrum [2]–[4], [16]–[18]. Furthermore, a hybrid of multiple lamp source types is proposed to produce more complex spectrum [19].

For optical path, nonimaging optics technologies are widely employed in the design stage for uniform illumination systems. Ulbricht spherical chamber [20], [21] and its related structure [22] are adopted to provide uniform illumination. Parabolic mirrors [23], [24] and Fresnel lens [15], [25] are commonly applied to generate collimated beam. Freeform surfaces are widely employed to generate uniform flux due to its versatility performance [1], [26], [27].

Taking thermal dissipation into consideration, this paper proposes an ellipsoid-spherical combined system structure to provide uniform illumination and color mixing for photonic or photovoltaics device testing applications. The system mainly consists in two parts: ellipsoidal reflector and spherical chamber. Ellipsoidal surfaces which are usually applied in light concentrating systems [13], [28]–[30] are now used as the primary reflectors to collect rays from different sources. The spherical chamber works as secondary surface to provide uniform flux and mix spectrum. At the design stage of the system, algebraic equations are derived to evaluate the slot size on the conjugate plane of the primary reflector and further determine input slot on the secondary chamber. Then, relationship between uniformity and output slot size is also investigated by Monte Carlo (MC) ray tracing method. Furthermore, Finite element analysis results are employed to analyze heat distribution of the system. A prototype is fabricated to demonstrate the thermal dissipation, illumination uniformity and color mixing can be achieved by the proposed structure.

2. Structure Design

2.1 Structure Description

As demonstrated in Fig. 1(a), the ellipsoid-spherical combined system is mainly composed of two parts: one or more ellipsoidal reflectors and a spherical chamber. The ellipsoidal reflectors are applied to collect rays emitted from light sources located at one of the focus and the concentrated rays enter the spherical chamber at the conjugate focus. If multiple reflectors are used for the purpose of either color mixing or flux enhancement, they should be distributed symmetrically about the system axis. The spherical cavity sprayed with diffuse coat is applied to generate uniform
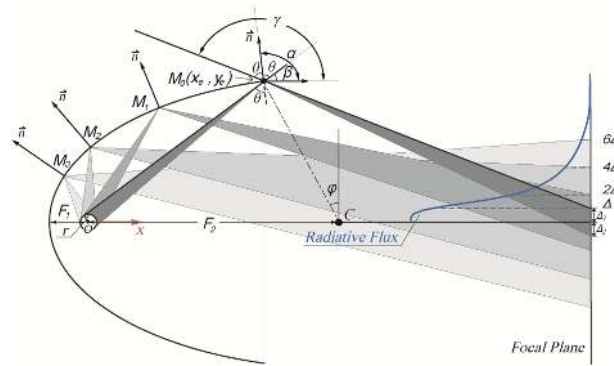
Fig. 2. Schematic of an ellipsoidal reflector and reflected rays from a volume source.

illumination and mix spectrum from different sources. Test plane is located in the opposite direction of the entry slot of light.

Fig. 1(b) demonstrates a prototype to verify the structure performance and the inset table shows its corresponding fabrication parameters. The spherical chamber is made of Acrylic plastic and coated with Barium Sulfate. In the paper, two types of light source are applied to the prototype: one ellipsoidal reflector with Xenon arc lamp is employed to study heat distribution and flux uniformity, while three ellipsoidal reflectors of multiple color LED sources are applied to study the color mixing capability.

2.2 Design Methods

2.2.1 Input Slot Size: As the input slot is located at the conjugate focus point of ellipsoidal reflector, it should be designed to allow more rays entering the chamber. Ideally, rays emitting from an ideal point light source at one focus of ellipsoid reflector would pass through the conjugate focus. In reality, enlarge of light source volume will cause light spot to spread on the conjugate focal plane, which requires designers to determine the input slot size on the chamber. Light distribution on the conjugate focal plane of the ellipsoidal reflector can either be simulated by either MC ray tracing simulation [31] or rigorous elliptical focusing formula based on spherical wave transformation [32]. Here, an approximation approach is proposed to estimate pattern size on the focal plane and thus decide input slot size, which is based on the 2D slice of the 3D ellipsoidal reflector and a uniformly emitting spherical source for discussion simplicity as shown in Fig. 2.

When rays from the source hit a given point on the ellipsoidal surface, $M(x_e, y_e)$ for example, the reflected rays follow the law of reflection and then passes through the conjugate focal plane, in which two factors require more attention. First, not all rays from the source can hit the point. The boundary between reachable and unreachable zone is decided by two lines passing through the point M and tangential to the source surface. Second, a bundle of rays reflected by a point with larger polar angle φ tends to diverge in the space and have sparser energy density on the conjugate focal plane. Thus, the rays reflected by M_0 at the output aperture point have the minimal size labeled as $\triangle$ on the conjugate plane. At the plane, rays come from both M_0 and other points of the reflector overlap at $\triangle$ region which make it have the highest flux across the region. Thus, find out $\triangle$ can help to estimate spot size.

To determine $\triangle$ from an ellipsoidal reflector described by equation (1), the polar angle φ is limited in (90°, 180°) for discussion simplify.

$$\frac{(x-c)^2}{a^2} + \frac{y^2}{b^2} = 1, \ c = \sqrt{a^2 + b^2} \tag{1}$$

As $\triangle$ is determined by the cross point of the conjugate focal plane ($x = 2c$) and the reflected tangential line. As there are two tangential lines from M_0 to the source, $\triangle$ has two main possible
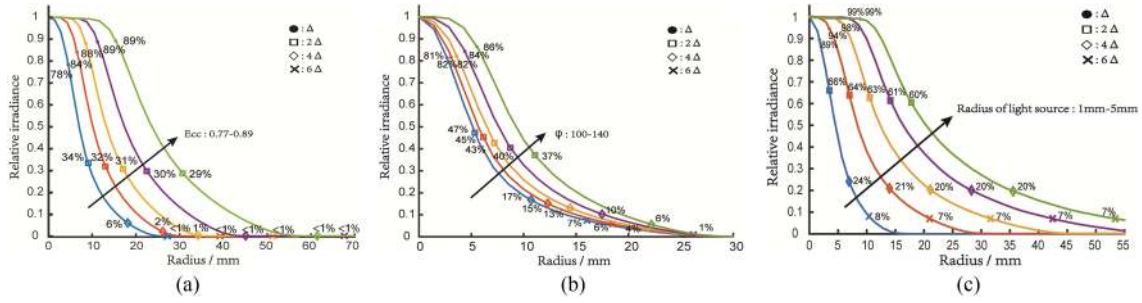
Fig. 3. Radial intensity distribution on the conjugate focal plane impacted by: (a) Eccentricity, (b) Aperture size, (c) Radius of light source. Separated mark: Positions calculated based on equations (2), (4), (6), and (7). Solid line: MC ray tracing.

values: Δ_1 and Δ_2. According to the geometric optics, the slope of angle α, β and then γ need to be determined first to find out Δ_1 and Δ_2.

As α is the incline angle of ellipse normal vector $[(x_e - c)/a^2, y_e/b^2]$ which can be calculated by the gradient of equation (1), its slope is determined by equation (2):

$$k_\alpha = \frac{y_e a^2}{(x_e - c)b^2},\tag{2}$$

in which, (x_e, y_e) is the coordinate of output aperture.

β is incline angle of tangential line which is written as $y - y_e = k_\beta(x - x_e)$. Furthermore, the distance between the line and circle center $O(0, 0)$ should equal to the circle radius r following equation (3):

$$\frac{y_e - k_\beta x_e}{\sqrt{1 + k_\beta{}^2}} = r.\tag{3}$$

Equation (3) has two roots as demonstrated by equation (4):

$$k_{\beta\pm} = \frac{-x_e y_e \pm r\sqrt{x_e{}^2 + y_e{}^2 - r^2}}{r^2 - x_e{}^2}.\tag{4}$$

Thus, the tilt angle γ of the reflected line can be calculated by $\gamma = \beta + 2\theta = 2\alpha - \beta$, and its slope can be determined by equation (5):

$$k_{\gamma\pm} = \tan(2\alpha - \beta)$$

$$= \frac{2k_\alpha - k_{\beta\pm} + k_{\beta\pm}k_\alpha{}^2}{1 - k_\alpha{}^2 + 2k_\alpha k_{\beta\pm}}.\tag{5}$$

Thus, the reflected line follows equation (6):

$$y = k_{\gamma\pm}(x - x_e) + y_e.\tag{6}$$

As Δ is determined by the reflected line and the conjugate focal plane, let $x = 2c$ in equation (6) and get the equation (7) to calculate Δ.

$$\Delta = \max(abs\{\Delta_1, \Delta_2\})$$

$$= \max(abs\{k_{\gamma\pm}(2c - x_e) + y_e\}).\tag{7}$$

By equations (2), (4), (6) and (7), it can be concluded that the ellipsoid structure parameters a, b (or c and eccentricity as optional), its aperture size and the light source size parameter r have impact on the spot size parameter Δ.

Fig. 3 demonstrates intensity distribution affected by above three groups of parameters simulated by MC ray tracing, and the calculated Δ values based on equation (2), (4), (6) and (7) are also
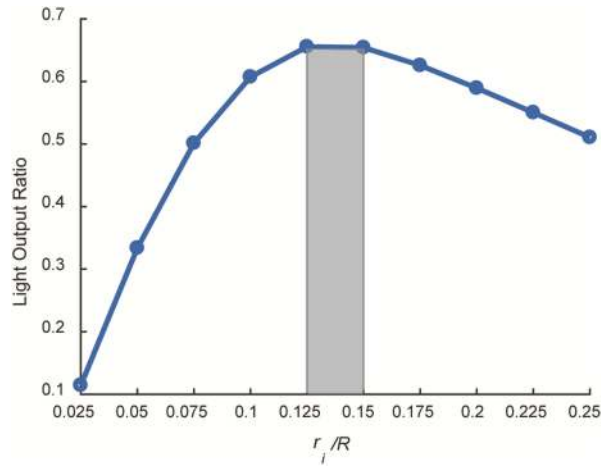
Fig. 4. Light output ratio varies with input slot size by MC ray tracing. R and ri are the radii of spherical chamber and input slot, respectively.
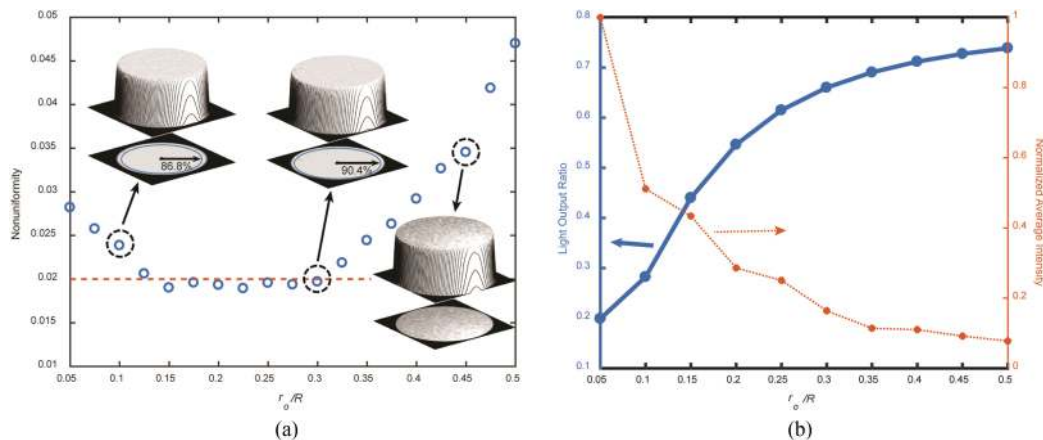

Fig. 5. Impact of output slot size on (a) nonuniformity; (b) light output ratio and normalized average intensity by MC ray tracing simulation. Insets: Intensity distribution on test plane and its corresponding 3D meshed pattern. R and ro are the radii of spherical chamber and output slot, respectively.

marked. Fig. 3 indicates that increase of the eccentric and the source radius as well as reduce the aperture size (controlled by parameter φ) would result in a larger spot on the conjugate plane. The variation rule is in accordance with the calculated result and indicates that region $\triangle$ has the highest flux concentration, which could be interest for concentrated simulator designers. For the proposed structure, it is suggested to make the input slot at least $6\triangle$ to collect more rays into the chamber, or the equations could also be adopted to decide light source size for a given system.

Light output ratio (*LOR*) is defined as luminous flux ratio between the luminaire and light sources, which are typically employed to describe efficiency of a luminaire. As shown in Fig. 4, if the input slot size is not large enough, a large amount rays will be blocking from entering the chamber, which results in a much lower *LOR*. However, if the input slot is too large, more energy will leak from the input instead of the output slot, which would also lead to a lower *LOR*. Therefore, the preferred input slot size based on structure parameters in Fig. 1(b) is between 12.5% and 15% of the spherical chamber, when considering all factors above.

2.2.2 Output Slot Size: Fig. 5(a) indicates that the spherical chamber outlet size has impact on the intensity uniformity, in which the uniformity variation across the 90% output slot is studied to
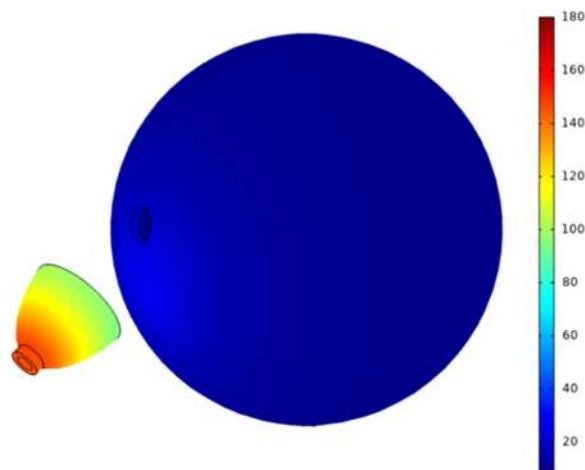
Fig. 6. Heat distribution according to finite element method simulation.

ignore the interference by slot edge. When the open slot is small, intensity can keep good uniformity around the slot center, but the uniformity will be affected largely by the slot edge. In this case, the 2% nonuniformity region, usually required for photovoltaic devices testing [33], is small which limits available test area. For larger output slot sizes, the function of the spherical chamber degrades, which leads to a rapid increase in nonuniformity. As a trade-off between the uniformity and available test space, a proposed output slot size is between 15% and 30% of the spherical chamber radius.

Fig. 5(b) demonstrates the impact of output slot size on output energy. The results show that a smaller output slot size is beneficial to provide higher illumination intensity, but the *LOR* is lower due to small outlet area. For a large outlet, the impact caused by the increasing area exceeds that by intensity reduction, which results in increase of the *LOR*. In this case, rays have higher probability to escape from the chamber before sufficient reflection, which results in less light attenuation but worse uniformity.

2.2.3 Heat Transfer: Accompanied by light emission, high power light sources always generate a large amount heat that can be transferred to key optical components mainly in three forms: conduction, convection or thermal radiation [28]. To reduce the adverse effects caused by heat, heat dissipation must be carefully designed especially for high flux systems [5], [8]. For internal contact sources, heat energy can directly transferred by conduction through medium with a temperature gradient.

As no direct contact, the separated structure is beneficial to heat dissipation and finite element method simulation is applied to analyze temperature distribution (as shown in Fig. 6). Apparently, heat distribution is related to spatial position to the light source. Due to closer distance, the highest temperature is mainly located at the region between focus and vertex of the ellipsoidal reflector. Since separation of the two components, heat transfer to the spherical cavity is primarily due to thermal radiation and convection through air, so that temperature distribution on the spherical chamber is much lower.

3. Experiment and Results

3.1 Heat Distribution

To study heat distribution of the system, a 150 watt Xenon arc lamp is selected as the light source of the prototype as demonstrated in Fig. 1(b) and thermal images are captured every 2 minutes from 1 to 11 minute as shown in Fig. 7. For the prototype, temperature tends to be stabilized after 9 minutes. The highest temperature on the ellipsoidal reflector varies from 71.2 °C at 1 minute to
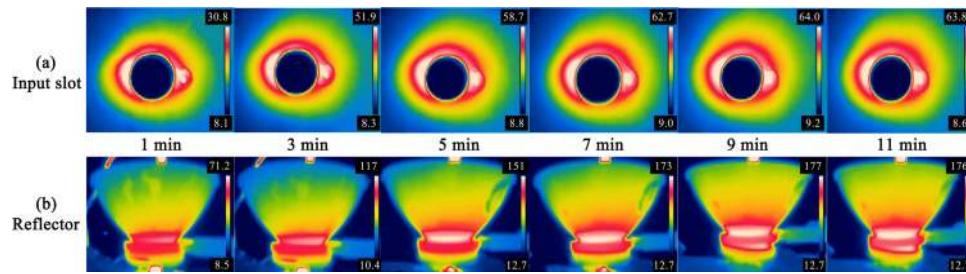
Fig. 7. Thermal image of the prototype illuminated by a 150 watt Xenon arc lamp.
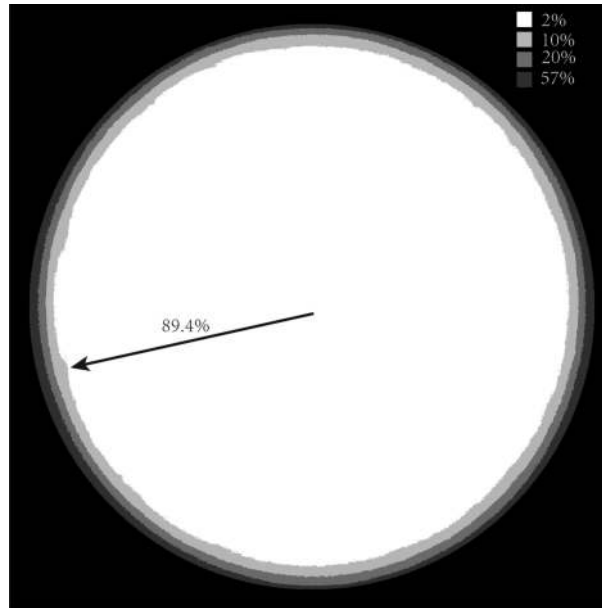

Fig. 8. Contour map of nonuniformity distribution on test plane illuminated with a 150 watt Xenon arc lamp.

around 176 °C after 9 minutes, which is accordance with the simulation results. For the spherical chamber, there is a high temperature region distributed around the inlet (from 30.8 °C to about 64 °C during the studying time), which is mainly due to absorption of the light and not been considered in the simulation. Although higher radiation flux would lead to a higher temperature, most energy is located at the center of the incident converging beam and the intensity decrease fast along the radial direction at the conjugate focal plane of the reflector. Impact of light absorption is limited in a small region and most part of the chamber surface can still keep as the environment temperature. Thus, the separated structure is helpful to heat dissipation and improve thermal stability for the system.

3.2 Uniformity

Fig. 8 demonstrates contour map for intensity distributed on the test plane illuminated by the 150 watt Xenon arc lamp. Within 89.4% of the output slot radius, the nonuniformity is controlled in the 2% requirement. However, the uniformity drops rapidly when approaching the output slot edge, which indicates that the edge has significant impact on the uniformity and thus sample under test should be placed close to the output center in practical applications.
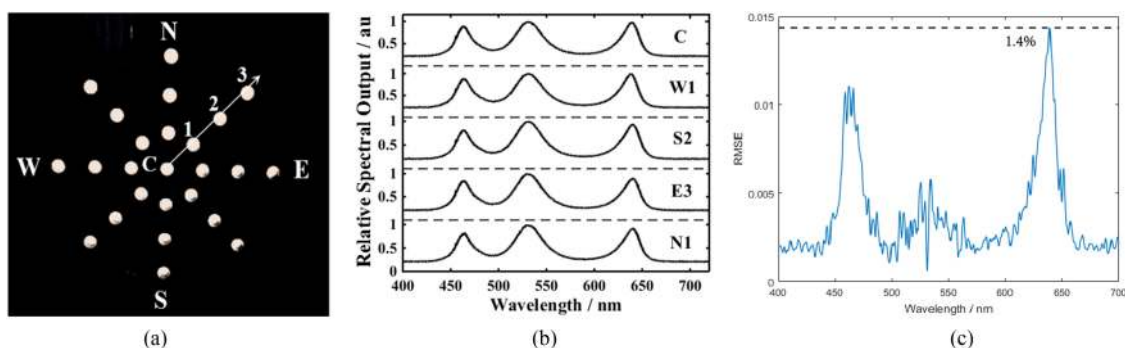
Fig. 9. Color mixing of the prototype illuminated by red, green, and blue LEDs: (a) sampling positions distributed at 90% of the output slot, (b) example spectrum at some of the positions, (c) RMSE across the sampling positions.

3.3 Color Mixing

Color mixing approaches are generally used by designers to fit more complex spectrum by multiple light sources. Generally, elaborately planning of the spatial position for lamps [16], [19] freeform lens [4] and light guide design [34] is widely approach to provide color mixing. One of the advantages of the proposed structure is that it simplifies the spatial position optimization process in color mixing system design, in which designers could focus more on source parameter selection and then place the sources at the focus of one or more symmetric distributed ellipsoidal reflectors.

As the structure has less dependency with light source type, three LEDs with red, green and blue colors placed in three ellipsoidal reflectors are employed to study color mixing capability for the prototype. As shown in Fig. 9(a), 25 sample positions distributing on the 90% radius of the output slot are employed to verify the spectrum consistency, in which the maximum root mean square error (*RMSE*) is 1.4% as demonstrated in Fig. 9(c).

4. Conclusions

In this paper, an ellipsoid-spherical combined system structure is proposed for uniform illumination and color mixing which is mainly divided into the ellipsoidal reflectors to collect rays and spherical chamber to generate uniform flux and mix spectrum. Furthermore, suggestions about input and output slot size optimization are presented. For input slot size, algebraic equations to estimate the spot size on the conjugate focus plane of the ellipsoid reflector is derived and further applied to decide the inlet size on sphere chamber, which reveals that it has relationship with size of light sources as well as shape, aperture of the ellipsoidal reflectors. For the input slot, a smaller opening size will block rays from entering chamber and a larger size will cause energy leak, which will all result in a lower *LOR*. Therefore, the preferred input slot size for prototype in the paper is between 12.5% and 15% of the spherical chamber radius. For outlet on spherical chamber, MC ray tracing simulation suggests that the most preferable output slot size of the structure is between 15% and 30% of the spherical chamber radius, when considering both uniformity and available test size. Simulation also suggests that a smaller output slot can provide higher illumination intensity and lower *LOR*, while a larger one has the opposite situation.

Based on the principles, a prototype is implemented to verify the performance for the structure. Experiment demonstrates that the systems tends to thermal stable after 9 minutes illumination under a 150 watt Xenon arc lamp and a temperature gradient distribution field on the ellipsoidal reflector is up to 178 °C which is in accordance with the finite element simulation. Considering light absorption by the spherical chamber material, the highest temperature distributes around a small area of the input slot and most part of the chamber keeps much lower temperature, which is beneficial the system heat stability. Under illumination with the same lamp, the 2% nonuniformity is

reached in 89.4% of the output slot size. Three LED sources with red, green and blue colors are applied to test color mixing capability of the system. The result reveals that the maximum *RMSE* is 1.4% across 90% of the test plane. Therefore, for applications such as photonic or photovoltaics device testing, the proposed structure is a candidate to generate uniform flux and color mixing with simplified optical path design, and it is also promising to meet heat dissipation requirements.

References

[1] R. Zhu, Q. Hong, H. Zhang, and S. Wu, "Freeform reflectors for architectural lighting," *Opt. Exp.*, vol. 23, pp. 31828–31837, 2015.

[2] Z. Zhu, X. Jin, H. Yang, and L. Zhong, "Design of diffuse reflection freeform surface for uniform illumination," *J. Display Technol.*, vol. 10, pp. 7–12, 2014.

[3] T. W. Sawyer, A. S. Luthman, and S. E. Bohndiek, "Evaluation of illumination system uniformity for wide-field biomedical hyperspectral imaging," *J. Opt.*, vol. 19, pp. 1–10, 2017.

[4] A. Teupner, K. Bergenek, R. Wirth, P. Benítez, and J. C. Miñano, "Color uniformity in spotlights optimized with reflectors and TIR lenses," *Opt. Exp.*, vol. 23, pp. A118–A123, 2015.

[5] E. Chen, R. Wu, and T. Guo, "Design a freeform microlens array module for any arbitrary-shape collimated beam shaping and color mixing," *Opt. Commun.*, vol. 321, pp. 78–85, 2014.

[6] A. Martin, N. Bordel, C. Blanco, J. Carlos, A. Anton, and G. Zissis, "Comparison of the emission of a high-pressure sodium lamp working at 50 Hz and at high frequency," *IEEE Trans. Ind. Appl.*, vol. 46, no. 5, pp. 1740–1745, Sep./Oct. 2010.

[7] F. Aksoy, H. Karabulut, C. Çınar, H. Solmaz, Y. Ö. Özgören, and A. Uyumaz, "Thermal performance of a stirling engine powered by a solar simulator," *Appl. Thermal Eng.*, vol. 86, pp. 161–167, 2015.

[8] Y. Li, S. Liu, and A. Shukla, "Experimental analysis on use of thermal conductivity enhancers (TCEs) for solar chimney applications with energy storage layer," *Energy Build.*, vol. 116, pp. 35–44, 2016.

[9] S. A. Gevorgyan, J. E. Carlé, R. Søndergaard, T. T. Larsen-Olsen, M. Jørgensen, and F. C. Krebs, "Accurate characterization of OPVs: Device masking and different solar simulators," *Sol. Energy Mater. Sol. Cells*, vol. 110, pp. 24–35, 2013.

[10] D. S. Codd, A. Carlson, J. Rees, and A. H. Slocum, "A low cost high flux solar simulator," *Sol. Energy*, vol. 84, pp. 2202–2212, 2010.

[11] X. Dong, Z. Sun, G. J. Nathan, P. J. Ashman, and D. Gu, "Time-resolved spectra of solar simulators employing metal halide and xenon arc lamps," *Sol. Energy*, vol. 115, pp. 613–620, 2015.

[12] Q. Meng, Y. Li, and Y. Gu, "Dynamic mesh-based analysis of dynamic irradiance characteristics of solar simulator," *Optik*, vol. 126, pp. 4658–4664, 2015.

[13] J. Petrasch *et al.*, "A novel 50 kW 11,000 suns high-flux solar simulator based on an array of xenon arc lamps," *J. Sol. Energy Eng.*, vol. 129, pp. 405–411, 2006.

[14] W. Wang, L. Aichmayer, B. Laumert, and T. Fransson, "Design and validation of a low-cost high-flux solar simulator using Fresnel lens concentrators," *Energy Procedia*, vol. 49, pp. 2221–2230, 2014.

[15] J. Li, J. G. Aguilar, C. P. Rábago, H. Zeaiter, and M. Romero, "Optical analysis of a hexagonal 42 kWe high-flux solar simulator," *Energy Procedia*, vol. 57, pp. 590–596, 2014.

[16] M. Stuckelberger *et al.*, "Class AAA LED-based solar simulator for steady-state measurements and light soaking," *IEEE J. Photovolt.*, vol. 4, no. 5, pp. 1282–1287, Sep. 2014.

[17] B. H. Hamadani *et al.*, "Towards realization of a large-area light-emitting diode-based solar simulator," *Prog. Photovolt.*, vol. 21, pp. 779–789, 2013.

[18] T. Nakajima, K. Shinoda, and T. Tsuchiya, "Single-LED solar simulator for amorphous Si and dye-sensitized solar cells," *RSC Adv.*, vol. 4, pp. 19165–19171, 2014.

[19] G. Grandi, A. Ienina, and M. Bardhi, "Effective low-cost hybrid LED-halogen solar simulator," *IEEE Trans. Ind. Appl.*, vol. 50, no. 5, pp. 3055–3064, Sep./Oct. 2014.

[20] A. Rehman, A. G. Anwer, and E. M. Goldys, "Programmable LED-based integrating sphere light source for wide-field fluorescence microscopy," *Photodiagnosis Photodyn. Ther.*, vol. 20, pp. 201–206, 2017.

[21] A. Kaehler and G. Bradski, "Integrating point source for texture projecting bulb," U.S. Patent 0 356 620 A1, Dec. 14, 2017.

[22] C. Yang, J. Wang, X. Guo, Y. Wang, and Zhao Ding, "A multisource regular dodecahedron solar simulator structure for uniform flux," *IEEE J. Photovolt.*, vol. 6, no. 2, pp. 516–521, Mar. 2016.

[23] B. Erickson and J. Petrasch, "Inverse identification of intensity distributions from multiple flux maps in concentrating solar applications," *J. Phys., Conf. Ser.*, vol. 369, no. 1, 2012, Art. no. 012014.

[24] G. Xiao, K. Guo, Z. Luo, M. Ni, Y. Zhang, and C. Wang, "Simulation and experimental study on a spiral solid particle solar receiver," *Appl. Energy*, vol. 113, pp. 178–188, 2014.

[25] W. Wang, L. Aichmayer, J. Garrido, and B. Laumert, "Development of a Fresnel lens based high-flux solar simulator," *Sol. Energy*, vol. 144, pp. 436–444, 2017.

[26] C. Tsai and B. Wang, "A freeform mirror design of uniform illumination in streetlight from a split light source," *IEEE Photon. J.*, vol. 10, no. 4, Aug. 2018, Art. no. 2201212.

[27] S. Li, F. Chen, K. Wang, S. Zhao, Z. Zhao, and S. Liu, "Design of a compact modified total internal reflection lens for high angular color uniformity," *Appl. Opt.*, vol. 51, pp. 8557–8562, 2012.

[28] R. Gu, J. Ding, Y. Wang, Q. Yuan, W. Wang, and J. Lu, "Heat transfer and storage performance of steam methane reforming in tubular reactor with focused solar simulator," *Appl. Energy*, vol. 233/234, pp. 789–801, 2019.

[29] J. Garrido, L. Aichmayer, W. Wang, and B. Laumert, "Characterization of the KTH high-flux solar simulator combining three measurement methods," *Energy*, vol. 141, pp. 2091–2099, 2017.

[30] J. Sarwara, G. Georgakis, R. L. Chance, and N. Ozalp, "Description and characterization of an adjustable flux solar simulator for solar thermal, thermochemical and photovoltaic applications," *Sol. Energy*, vol. 100, pp. 179–194, 2014.

[31] X. Dong, G. J. Nathan, Z. Sun, D. Gu, and P. J. Ashman, "Concentric multilayer model of the arc in high intensity discharge lamps for solar simulators with experimental validation," *Sol. Energy*, vol. 122, pp. 293–306, 2015.

[32] J. Liu, J. Tan, T. Wilson, and C. Zhong, "Rigorous theory on elliptical mirror focusing for point scanning microscopy," *Opt. Exp.*, vol. 20, pp. 6175–84, 2012.

[33] "Photovoltaic devices: Part 9: Solar simulator performance requirements," IEC, Geneva, Switzerland, IEC 60904-9, 2nd ed., 2007.

[34] C. Sun, I. Moreno, Y. Lo, B. Chiu, and W. Chien, "Collimating lamp with well color mixing of red/green/blue LEDs," *Opt. Exp.*, vol. 20, pp. A75–A84, 2014.